Int J Adv Manuf Technol
DOI 10.1007/s00170-017-0877-x

ORIGINAL ARTICLE

# Novel analytical and experimental trajectory optimization of a 7-DOF baxter robot: global design sensitivity and step size analyses

Mostafa Bagheri[1] · Peiman Naseradinmousavi[1]

Received: 27 March 2017 / Accepted: 24 July 2017

**Abstract** In this paper, we present a novel nonlinear analytical coupled trajectory optimization of a 7-DOF Baxter manipulator validated through experimental work utilizing global optimization tools. The robotic manipulators used in network-based applications of industrial units and even homes, for disabled patients, spend significant lumped amount of energy and therefore, optimal trajectories need to be generated to address efficiency issues. We here examine both heuristic (Genetics) and gradient-based (GlobalSearch) algorithms for a novel approach of "S-Shaped" trajectory (unlike conventional polynomials), to avoid being trapped in several possible local minima along with yielding minimal computational cost, enforcing operational time and torque saturation constraints. The global schemes are utilized in minimizing the lumped amount of energy consumed in a nominal path given in the collision-free joint space except an impact between the robot's end effector and a target object for the nominal operation. Note that such robots are typically operated for thousands of cycles resulting in a considerable cost of operation. Due to the expected computational cost of such global optimization algorithms, step size analysis is carried out to minimize both the computational cost (iteration) and possibly cost function by finding an optimal step size. Global design sensitivity analysis is also performed to examine the effects of changes of optimization variables on the cost function defined.

**Keywords** Robotics · Joint-space optimization · Step size analysis · Global sensitivity analysis · Experimental validation

## 1 Introduction

Autonomous and nonautonomous operations of any electromechanical system, in particular robots, have received considerable attention with respect to both the stability and, more importantly, efficiency issues. Both the autonomous and nonautonomous methods, which utilize online and offline/blind optimization and control schemes, respectively, have revealed some advantages and disadvantages. We here focus on the nonautonomous energy-efficient operation of the Baxter manipulator which would subsequently be used in nonlinear control schemes as desirable trajectories. The offline optimization/control of the robot will be gradually examined with respect to the autonomous practice to yield the most reliable and optimal configuration.

Note that the robots are widely utilized in industry due to their reliable, fast, and precise motions [11] although they are not energy efficient and hence consume a significant lumped amount of energy. The energy consumption and subsequently cost of operation considerably increase when thousands of the robots work together, for example in a factory, to carry out a network-based task for thousands of cycles. Based on the recent statistics published, manufacturing industries are among the largest consumers of energy in which the robots they employ take the biggest share of

✉ Peiman Naseradinmousavi
pnaseradinmousavi@mail.sdsu.edu;
peiman.n.mousavi@gmail.com

Mostafa Bagheri
mbagheri@sdsu.edu

[1] Dynamic Systems and Control Laboratory (DSCL),
Department of Mechanical Engineering, San Diego State
University, San Diego, CA 92115, USA

Published online: 03 August 2017

consumption [29]. It is worthy to mention that the robots used in auto industry consume more than half of the total energy required to produce a vehicle body.

The importance of the optimal operation can be visualized through a network of robots operating simultaneously to carry out a specific task defined; we have reported another effort of the interconnected operational optimization in [36] for the so-called "Smart Valves Network" [33–35]. The robot manipulator, which is being analyzed in this research work, is operated for thousands of cycles in industries and even homes as a reliable servant for disabled patients. A considerable lumped amount of energy is expectedly consumed in a nominal trajectory given, as a part of the network-based operation, and it hence needs to be minimized resulting in a significant reduction of operational cost.

Therefore, the issue of energy consumed by robots has become a major challenge for researchers and robot manufacturers [1–3, 6, 9, 10, 16, 19–25, 27, 28, 31, 37, 39, 41–43, 48–50, 52, 53, 55, 57]. The total mechanical energy consumed by the robot is expectedly affected by the required torque of each joint in addition to the joints' angular velocities. The high level of energy consumption is typically caused by jerky motions of robots. Many researchers have mainly focused on the optimal design of robots [5, 14, 26], path planning [17, 18, 30], and minimizing joints' torques [15, 54]. The geometrical constraints [32], dynamic characteristics, energy consumed, and execution time [40] are important issues which have been thoroughly addressed by researchers to carry out optimization. Many efforts have been reported in presenting optimal control schemes to optimize operation time and energy consumption [45, 46, 51]. Nevertheless, the most approaches have focused on minimizing the execution time, which may not necessarily yield a minimal amount of energy consumption [7, 8, 12, 38]. From another aspect, the robot redundancy yields motion dexterity which in turn would avoid harmful singularities and potentially workspace obstacles. We have previously reported [5] the effects of redundancy on the design optimization process.

Note that the operational optimization scheme, which is being formulated here, needs three phases to be carried out. First, we have a collision-free nominal trajectory which will be discussed in detail except a collision between the robot's end effector and a target object due to the jerky motion of the nominal operation. Based on the assumption of collision-free motion, adding more points between the initial and end points makes no sense and expectedly only imposes significant computational cost by implementing conventional polynomials of Spline and Beźier which contain considerable additional constraints; this would lead to tedious and gradually infeasible computational burden for such a 7-DOF robot. Therefore, the contribution of this work is to propose novel "S-Shaped" trajectories to overcome the difficulties mentioned earlier. Then, the cost function is formulated as the lumped amount of mechanical energy consumption enforcing operational time and torque saturation constraints. Finally, we utilize global optimization schemes, the heuristic and gradient-based ones, in improving the dynamic characteristics of a given nominal trajectory along with minimizing the energy consumption.

After deriving fourteenth-order dynamic equations using the Lagrangian method, the results of experimental work are presented to examine the accuracy of the modeling process. We then utilize both the Genetic and GlobalSearch (gradient-based method) algorithms to avoid being trapped in several possible local minima with respect to the bounds of optimization variables, which are determined based on the operational time and torque saturation constraints. Optimization of such interconnected nonlinear coupled equations needs step size analysis to improve an expected cumbersome computational cost (iteration). An optimal step size is numerically calculated to avoid a significant computational cost/time. The effects of changes of optimization variables on the cost function defined are also studied using global design sensitivity analysis. The gradient of cost function is calculated with respect to the optimization variables to reveal the share of each variable in minimizing the lumped energy consumption.

## 2 Mathematical modeling

The redundant manipulator, which is being studied here, has 7-DOF as shown in Fig. 1. The mass, Coriolis, and

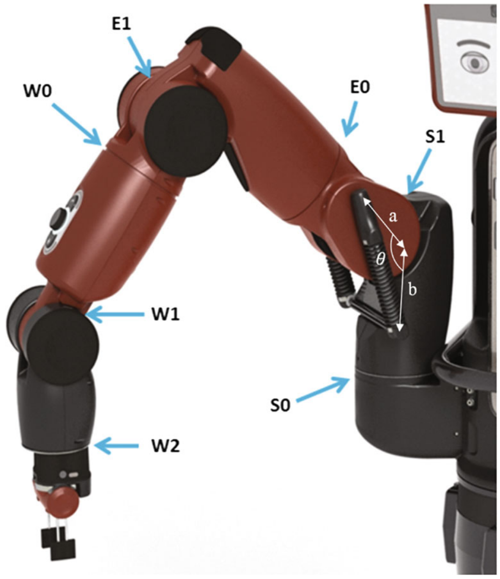

**Fig. 1** The 7-DOF Baxter's arm

**Table 1** Baxter's Denavit-Hartenberg parameters

| Link | $a_i$ | $d_i$ | $\alpha_i$ | $\theta_i$ |
|---|---|---|---|---|
| 1 | 0.069 | 0.27035 | $-\pi/2$ | $\theta_1$ |
| 2 | 0 | 0 | $\pi/2$ | $\theta_2 + \pi/2$ |
| 3 | 0.069 | 0.36435 | $-\pi/2$ | $\theta_3$ |
| 4 | 0 | 0 | $\pi/2$ | $\theta_4$ |
| 5 | 0.010 | 0.37429 | $-\pi/2$ | $\theta_5$ |
| 6 | 0 | 0 | $\pi/2$ | $\theta_6$ |
| 7 | 0 | 0.3945 | 0 | $\theta_7$ |

gravitational (stiffness) matrices are symbolically derived using the Euler-Lagrange equation. The robot's Denavit-Hartenberg and dynamic parameters are shown in Tables 1 and 2, respectively, provided by the manufacturer. In general, the Euler-Lagrange equation expectedly leads to a set of $n$ second-order ordinary differential equations:

$$\frac{d}{dt}\frac{\partial L}{\partial \dot{q}_i} - \frac{\partial L}{\partial q_i} = \tau_i \qquad i = 1, \cdots, n \tag{1}$$

where $L$ denotes the Lagrangian and is obtained based on kinetic and potential energies ($L = K - P$). The kinetic energy of an $n$-link manipulator, which has $n$ degrees of freedom, is a quadratic term of $\dot{q}$ (the vector of joints' angular velocities) as follows:

$$\begin{aligned} K &= \frac{1}{2}\dot{q}^T \sum_{i=1}^{n} [m_i J_{v_i}(q)^T J_{v_i}(q) \\ &\quad + J_{\omega_i}(q)^T R_i(q) I_i R_i(q)^T J_{\omega_i}(q)]\dot{q} \\ &= \frac{1}{2}\dot{q}^T D(q)\dot{q} = \frac{1}{2}\sum_{i,j}^{n} d_{ij}(q)\dot{q}_i\dot{q}_j \end{aligned} \tag{2}$$

where $J_{v_i}$ and $J_{\omega_i}$ are $3 \times n$ matrices making the Jacobian of mass center of $i$-th link and $n \times n$ "inertia matrix" ($D(q)$) is symmetric/positive definite for each $q \in \Re^n$.

Note that the Baxter's arm has a set of springs (Fig. 1) acting as a damper to absorb harmful vibration of the jerky motions as discussed earlier. The potential energy is hence obtained as the sum of both the gravitational and elastic (spring) terms as follows:

$$\begin{aligned} P &= \sum_{i=1}^{n} P_i + \frac{1}{2}k_{eq}x^2 \\ &= \sum_{i=1}^{n} g^T r_{c_i} m_i + \frac{1}{2}k_{eq}x^2 \end{aligned} \tag{3}$$

where $P_i$ is the potential energy of the $i$-th link, $g$ is the gravitational acceleration, $r_{c_i}$ indicates the coordinate of mass center of link $i$, $k_{eq}$ stands for the stiffness of preloaded springs in joint $S_1$, and $x$ is the spring displacement which is calculated as follows:

$$x = \sqrt{a^2 + b^2 - 2abcos(\theta)} \tag{4}$$

where $\theta = \frac{\pi}{2} + \psi$ ($\psi = -q_2$) as shown in Figs. 1 and 2. Using the energy terms presented in Eqs. 2 and 3, the general form of the Euler-Lagrange equation becomes as follows:

$$D(q)\ddot{q} + C(q,\dot{q})\dot{q} + \phi(q) = \tau \tag{5}$$

**Table 2** The Baxter's dynamic parameters

| Link | $m(kg)$ | $I_{xx}$ | $I_{yy}$ | $I_{zz}$ |
|---|---|---|---|---|
| 1 | 5.7005 | 0.047091 | 0.037669 | 0.035959 |
| 2 | 3.2269 | 0.011752 | 0.027885 | 0.020787 |
| 3 | 4.3127 | 0.026617 | 0.028443 | 0.012480 |
| 4 | 0.007116 | 2.07206 | 0.013182 | 0.009268 |
| 5 | 2.2466 | 0.016677 | 0.016754 | 0.003746 |
| 6 | 1.6097 | 0.003876 | 0.007005 | 0.005527 |
| 7 | 0.6747 | 0.005142 | 0.005455 | 0.006109 |

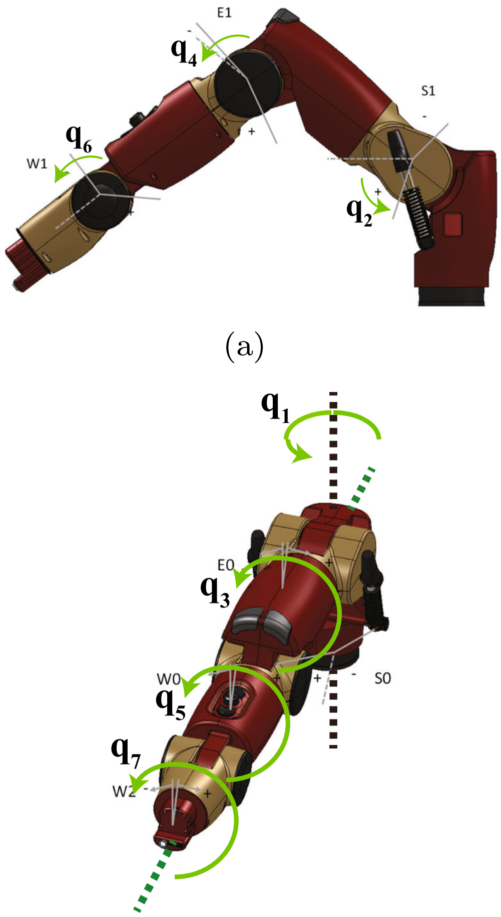

(a)

(b)

**Fig. 2** The joints' configuration. **a** Sagittal view. **b** Top view

where $\dot{q}$ and $\ddot{q}$ indicate the vectors of angular velocity and acceleration of the joints, respectively, $\tau$ is the driving torque vector, and $\phi(q)$ is the gravitational matrix as follows:

$$\phi_k = \frac{\partial P}{\partial q_k} \tag{6}$$

Utilizing the "Christoffel symbols" [47] would help us derive the elements of the Coriolis matrix ($C(q, \dot{q})$) as follows:

$$c_{ijk} = \frac{1}{2}\left\{\frac{\partial d_{kj}}{\partial q_i} + \frac{\partial d_{ki}}{\partial q_j} - \frac{\partial d_{ij}}{\partial q_k}\right\} \tag{7}$$

where the $k, j$-th element of $C(q, \dot{q})$ is calculated as follows:

$$\begin{aligned} c_{kj} &= \sum_{i=1}^{n} c_{ijk}(q)\dot{q}_i \\ &= \sum_{i=1}^{n} \frac{1}{2}\left\{\frac{\partial d_{kj}}{\partial q_i} + \frac{\partial d_{ki}}{\partial q_j} - \frac{\partial d_{ij}}{\partial q_k}\right\}\dot{q}_i \end{aligned} \tag{8}$$

We implemented the symbolic formulations in MATLAB and obtained the coupled fourteenth-order nonlinear dynamic equations to be used in the optimization process.

## 3 Experimental validation

The experimental validation of such a coupled nonlinear mathematical model is a necessity to be carried out in order to examine the accuracy of the formulation and then possibly refine the model. We hence recorded the joints' torques to be compared with the ones computed through the interconnected equations. The results are shown in Fig. 3a–d for four different joints which, in particular, need significant higher and lower amounts of torques, respectively, to be operated. Note that non-zero torques at the initial point, $t = 0$, stand for holding torques against gravity while the links are stationary leading to zero angular velocities/accelerations at the initial point.

Shown in Fig. 3a–d are the experimental and analytically computed nominal torques used in driving the joints $S_0$, $E_0$, $W_0$, and $W_1$, respectively, which reveal an acceptable consistency giving us the confidence to utilize the model developed in the optimization process. Note that the

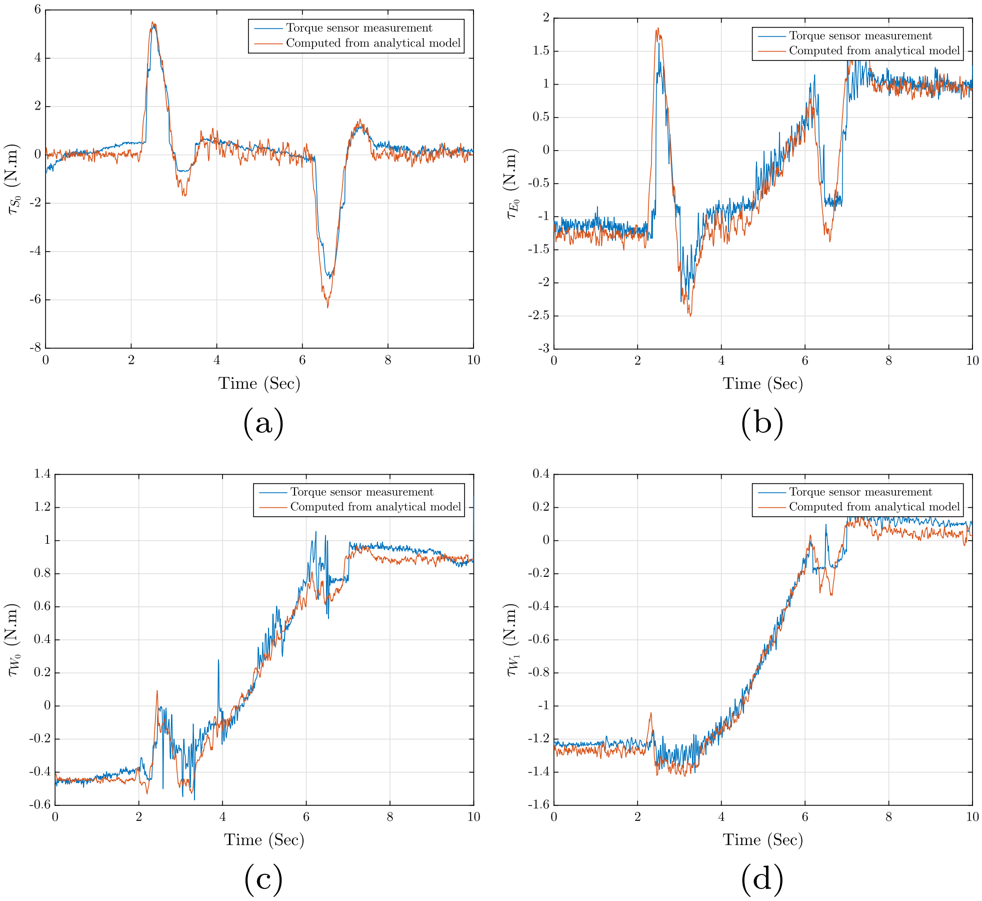

**Fig. 3** Comparison between the experimentally measured and nominal analytical torques used in driving the joints **a** $S_0$ and **b** $E_0$, **c** $W_0$ and **d** $W_1$; the non-zero torques at the initial point ($t = 0$) stand for holding torques against gravity

negligible differences potentially root on the unmodeled friction and backlash of the joints.

## 4 Trajectory optimization

The Baxter uses a simple PD controller and therefore, the lack of I controller has caused the jerky motions, steady state tracking errors, and subsequently inefficient operation of the robot. The undesirable responses can be observed through experimental work which we have carried out for a nominal trajectory in our **Dynamic Systems and Control Laboratory** (Fig. 3a–d). It can be observed that the robot collides with the target object. This is counted as a harmful dynamical behavior for both the industrial and home applications. Note that the Baxter, which is being analyzed here, has been designed for research purposes and hence has no predefined nominal trajectory. The robot operates using the PD controller with respect to the initial and end points given in the joints space, which in turn generates energy-inefficient trajectories. The coupled trajectory optimization of the robot, as a part of the nonautonomous approach, is a necessity to be carried out in order to considerably reduce the mechanical energy consumption along with removing the jerky motions to avoid such a harmful collision discussed earlier.

Note that the optimization needs to be formulated enforcing the operational time and torque saturation constraints to avoid the expected singularities. The feasible joints' ranges along with the initial and end points are listed in Table 3. One of the physical constraints, which needs to be implemented in the optimization formulation, is zero angular velocity/acceleration at the initial and zero angular velocity at the end points, indicating that the manipulator would remain stationary at those points: $\boxed{1}$ This constraint leads us to the well-known "S-Shaped" trajectories which would yield the robot's smooth dynamical behavior by mitigating the effects of jerky motions. Such a smooth trajectory obviously satisfies the initial/end points' zero angular velocity condition; $\boxed{2}$ The conventional polynomials, including Spline/Bézier ones, would yield considerably more variables to be optimized with respect to the joint-space optimization, which in turn would expectedly impose cumbersome computational costs. $\boxed{3}$ Note that adding points between the initial and end points only imposes additional constraints with cumbersome computational cost which would be meaningless with respect to the collision-free motion; except the collision between the robot's end effector and the target object for the nominal operation due to the jerky motion. Note that we have previously examined these trajectories (S-Shaped ones) for another interconnected electromechanical system [34] enforcing the geometrical and stability constraints [35]. We fit the following nonlinear functions (nominal trajectories) to the joints' real trajectories (shown in Figs. 5 and 6) which are generated with respect to the initial/end points given in Table 3 using the Baxter's PD controller:

$$\theta_i(t) = A_i \tanh(B_i t^{C_i}) + D_i \qquad i = 1, ..., 7 \tag{9}$$

where $A$'s, $B$'s, $C$'s, and $D$'s are calculated utilizing the least square method for the trajectory fitting process as listed in Table 4. Note that the $A$'s and $D$'s are constant/unique parameters for each joint and are easily calculated as *"End Points-Initial Points"* and *"Initial Points"*, respectively. The $B$'s and $C$'s are the optimization variables which are subject to the following lower and upper bounds determined through the following constraints:

$$\gamma_1 = [B_{1S_0}, B_{2S_1}, B_{3E_0}, B_{4E_1}, B_{5W_0}, B_{6W_1}, B_{7W_2}] \tag{10}$$

$$\gamma_{1min} = [88, 89, 88.5, 89, 86.5, 89.3, 89] \times 10^{-4} \tag{11}$$

$$\gamma_{1max} = [245, 261, 252, 248, 253, 260, 251] \times 10^{-4} \tag{12}$$

$$\gamma_2 = [C_{1S_0}, C_{2S_1}, C_{3E_0}, C_{4E_1}, C_{5W_0}, C_{6W_1}, C_{7W_2}] \tag{13}$$

$$\gamma_{2min} = [2.35, 2.19, 2.36, 2.27, 2.18, 2.35, 2.29] \tag{14}$$

$$\gamma_{2max} = [4.09, 4.2, 4.10, 4.20, 4.20, 4.30, 4.11] \tag{15}$$

The lower bound roots on the operational time indicating that the robot's motion will be within 12 s. Note that decreasing the lower bound would yield much slower motion which is not desirable and logical, in particular for the industrial applications. The upper bound is determined

**Table 3** The ranges of joints' angles (degree)

| Joint's name | Range | Initial point | End point |
|---|---|---|---|
| $S_0$ | −97.5 to 90 | −97.2070 | 29.5312 |
| $S_1$ | −80 to 60 | −71.1694 | −21.5338 |
| $E_0$ | −170 to 170 | −10.3052 | 0.1099 |
| $E_1$ | 0 to 150 | 46.9775 | 50.2954 |
| $W_0$ | −170 to 170 | −29.2676 | 35.7935 |
| $W_1$ | −90 to 115 | 19.1382 | 59.5459 |
| $W_2$ | −170 to 170 | −67.7417 | −156.9287 |

**Table 4** The nominal trajectories' coefficients

| Joint's name | A | B | C | D |
|---|---|---|---|---|
| $S_0$ | 126.7382 | 0.0172 | 2.6530 | −97.2070 |
| $S_1$ | 49.6356 | 0.0169 | 2.6480 | −71.1694 |
| $E_0$ | 10.4151 | 0.0171 | 2.6476 | −10.3052 |
| $E_1$ | 3.3179 | 0.0173 | 2.6390 | 46.9775 |
| $W_0$ | 65.0611 | 0.0168 | 2.6503 | −29.2676 |
| $W_1$ | 40.4077 | 0.0170 | 2.6410 | 19.1382 |
| $W_2$ | −89.187 | 0.0171 | 2.6515 | −67.7417 |

based on the Practical Torque Saturation issue such that increasing the upper bound would yield abrupt torques leading to both the motors' failures and considerably fast motion. The optimization problem is a constrained one, enforcing the mentioned lower and upper bounds, with the following cost function defined as the lumped amount of mechanical energy consumed in the robot for a predefined operational time:

$$\min E_{tot} = \sum_{i=1}^{7} \int_{0}^{t_f} \left| \tau_i \dot{\theta}_i \right| dt \tag{16}$$

Subject to :

The Interconnected Equations &

$$\gamma_{1min} \leq \gamma_1 \leq \gamma_{1max}$$

$$\gamma_{2min} \leq \gamma_2 \leq \gamma_{2max}$$

We hence need to optimize fourteen interconnected variables using global optimization schemes. Note that the variables are not of the same order, which resulted in serious numerical errors in our initial studies. We fixed this problem by conditioning them using a normalization scheme as follows:

$$\gamma_{1n} = \gamma_1 \times 10^4 \tag{17}$$

$$\gamma_{2n} = \gamma_2 \times 10^2 \tag{18}$$

We utilize two global optimization schemes, including genetic (GA) and GlobalSearch (GS) algorithms, to avoid being trapped in several possible local minima. The genetic method has been developed based on a heuristic search to mimic the process of natural selection [4, 13, 44, 56]. The genetic algorithm [34] is typically more robust than other conventional schemes. It does not break down easily in the presence of slight changes of inputs, and noise. For large-scale state-space equations, the algorithm may potentially exhibit significantly better performance than typical optimization techniques.

**Table 5** Optimal trajectories' coefficients

| Joint's name | GA | | GS | |
|---|---|---|---|---|
| | *B* | *C* | *B* | *C* |
| $S_0$ | 0.009 | 2.4 | 0.009 | 2.4 |
| $S_1$ | 0.025 | 4.0959 | 0.025 | 4.0999 |
| $E_0$ | 0.009 | 3.5250 | 0.009 | 3.5228 |
| $E_1$ | 0.0202 | 2.9073 | 0.0091 | 3.3691 |
| $W_0$ | 0.025 | 4.1 | 0.025 | 4.1 |
| $W_1$ | 0.0102 | 2.9273 | 0.009 | 3.0361 |
| $W_2$ | 0.0115 | 2.4 | 0.009 | 2.4001 |

The GlobalSearch method searches more through the possible trajectories, and computes the gradient of the cost function along with width step for finding new points. We have previously employed the GlobalSearch algorithm in Matlab [34] which uses gradient-based method to return local and global minima. The algorithm preliminary starts with a local solver (here fmincon) from multiple starting points and stores local and global solutions found during the search process. The fmincon solver estimates gradients utilizing parallel finite differences. Note that the global search solver uses a scatter-search pattern to generate multiple starting points which can be observed in figures shown in results section for presenting the gradient-based method. The function (TolFun) and constraints (TolCon) tolerances used in the GS scheme are $10^{-6}$.

Note that for the GA method we have utilized (1) "PopulationSizn of 200 for the size of population, (2) "Generations" of 140 which indicates the maximum number of iterations before the algorithm halts, (3) "MigrationFraction" of 0.2 specifying the fraction of individuals in each subpopulation that migrates to a different subpopulation, (4) "MigrationIntervan of 20 standing for the number of generations that take place between migrations of individuals between subpopulations, and (5) Function (TolFun) and constraints (TolCon) tolerances of $10^{-6}$.

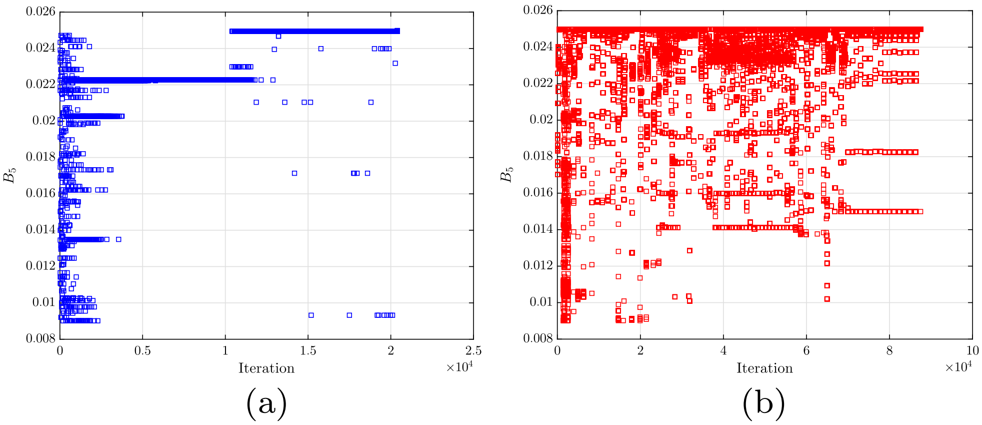

(a)

(b)

**Fig. 4** The optimized values of $B_5$ using **a** GA and **b** GS algorithms

**Fig. 5** The nominal and optimal trajectories using the GA and GS algorithms. **a** $S_0$. **b** $S_1$. **c** $E_0$

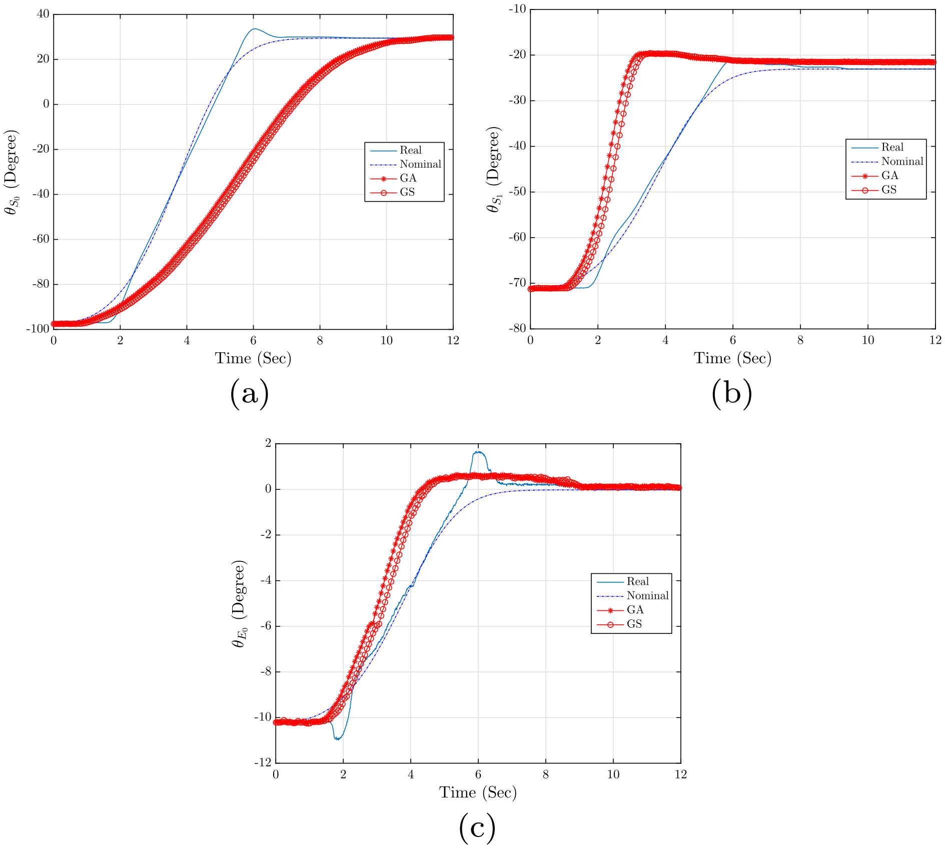

**Fig. 6** The nominal and optimal trajectories using the GA and GS algorithms. **a** $E_1$. **b** $W_0$. **c** $W_1$. **d** $W_2$

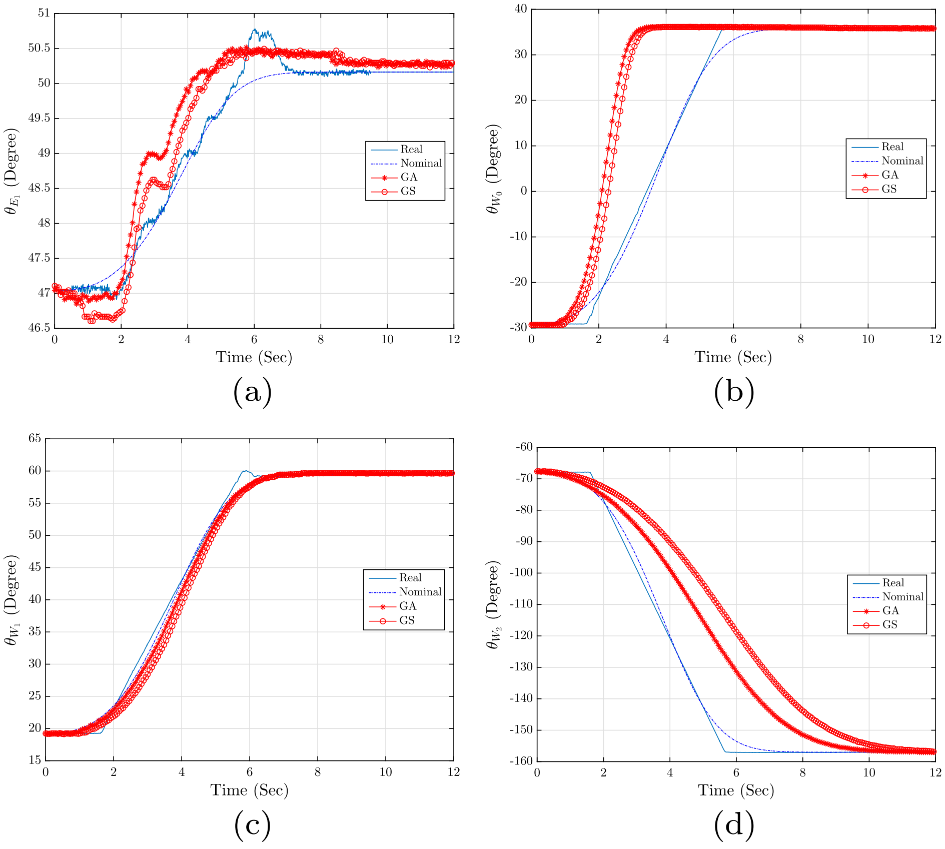

**Fig. 7** The global sensitivity analysis with respect to the B’s

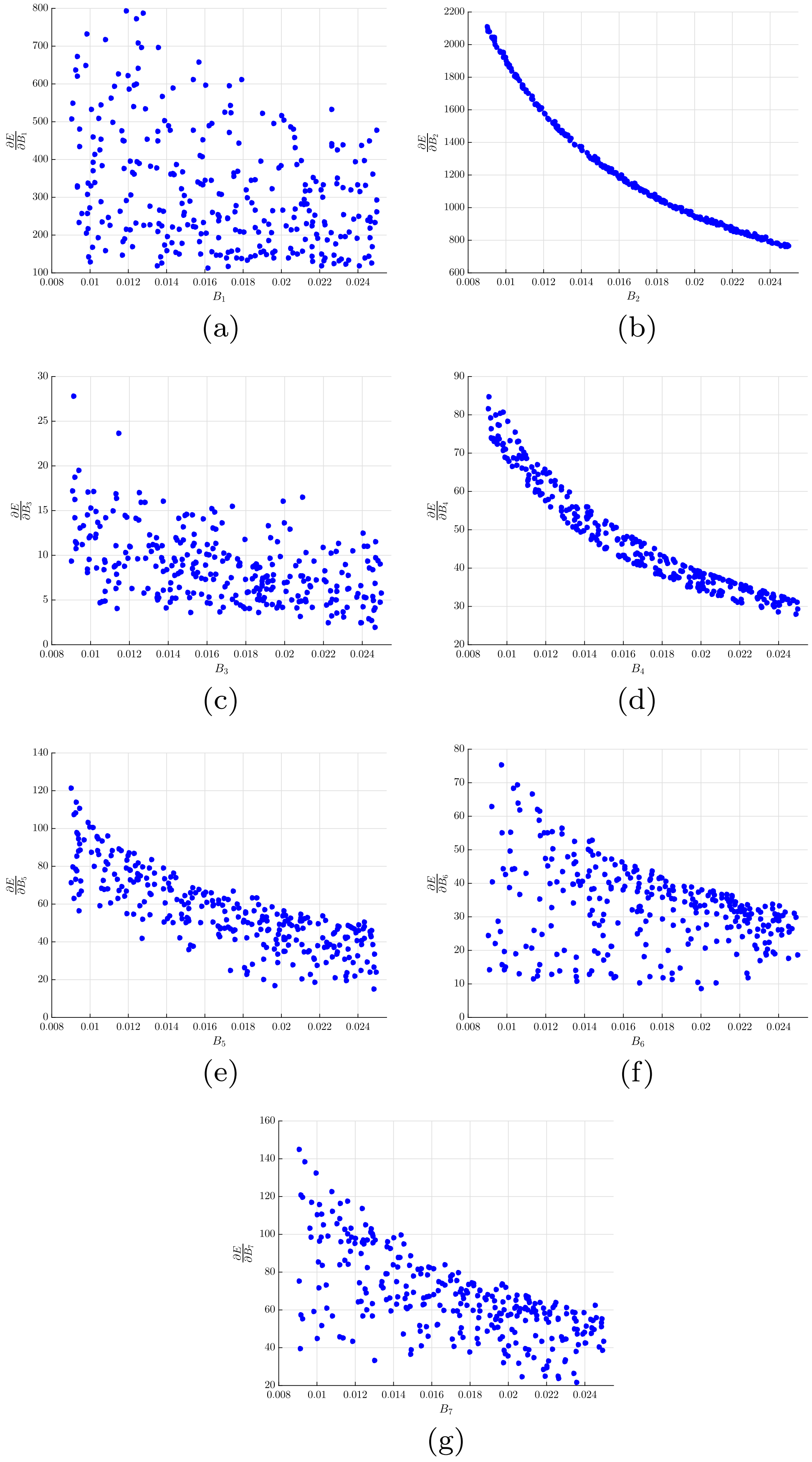

(a)

(b)

(c)

(d)

(e)

(f)

(g)

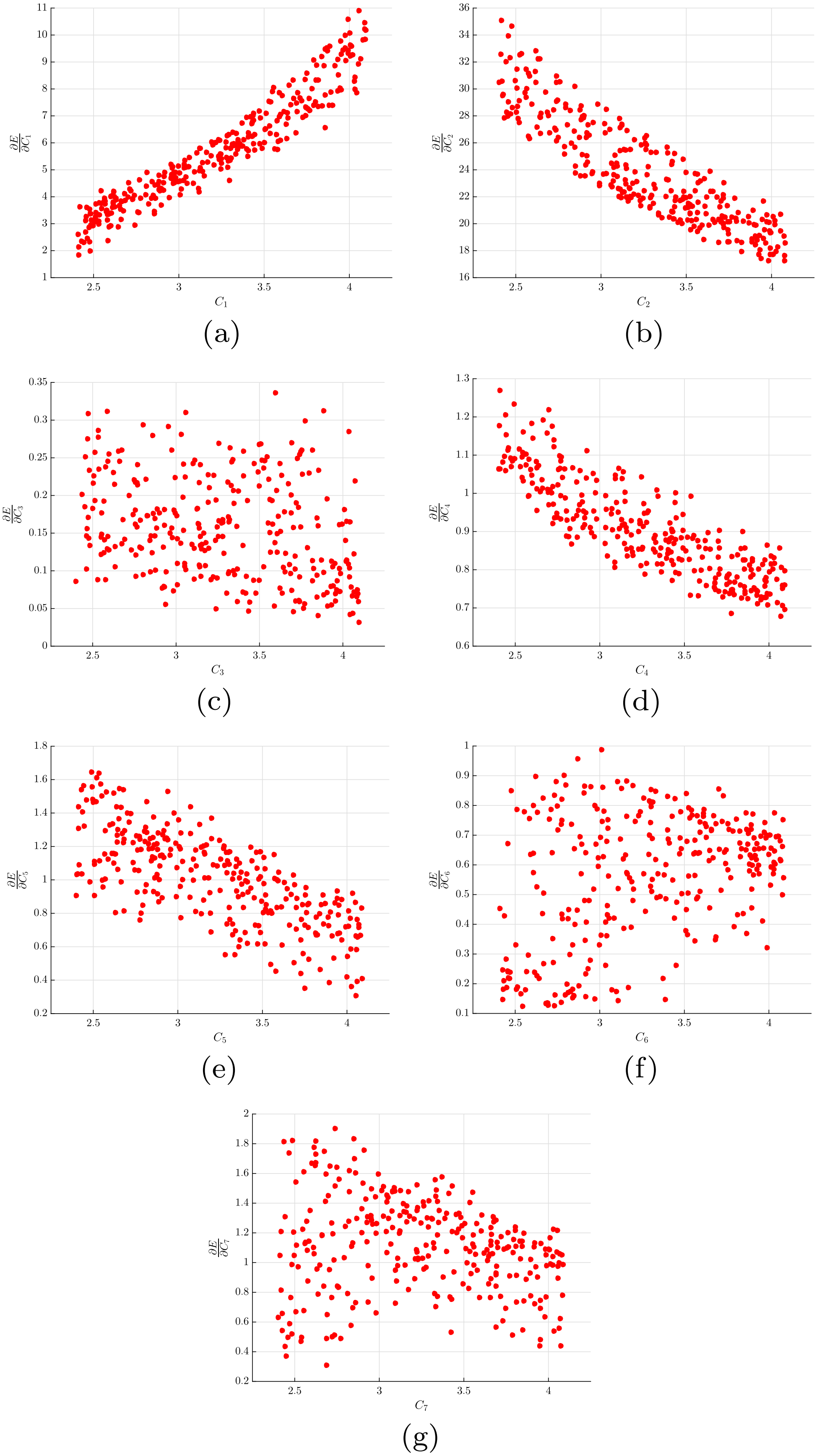

**Fig. 8** The global sensitivity analysis with respect to the C's

**Fig. 9** The energy optimized using **a** GA and **b** GS algorithms

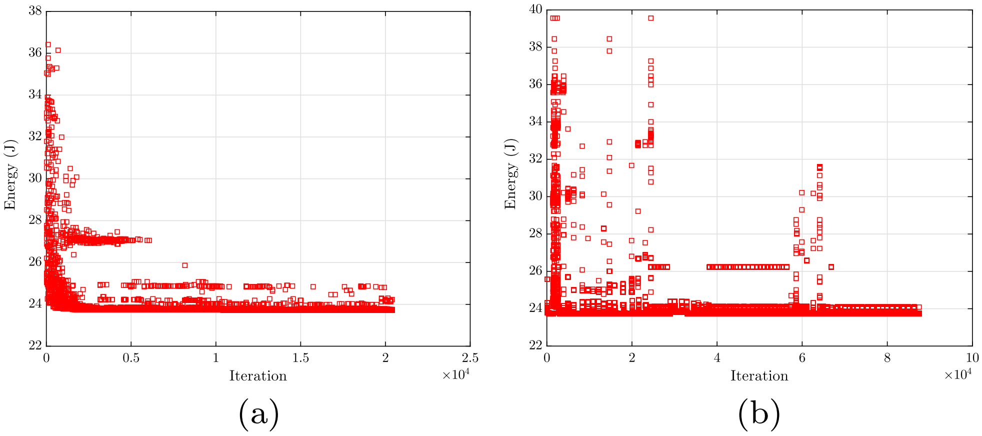

Note that the scatter-search pattern of the GS algorithm needs random initial guesses to be employed via the following formulations:

$$\gamma_{1rn} = \gamma_{1min} + (\gamma_{1max} - \gamma_{1min}) \times \mathrm{rand}(0,1) \quad (19)$$

$$\gamma_{2rn} = \gamma_{2min} + (\gamma_{2max} - \gamma_{2min}) \times \mathrm{rand}(0,1) \quad (20)$$

where rand (0,1) is a random number between zero and one. We implemented the algorithms in MATLAB and captured many interesting results.

## 5 Results

Figure 4 shows the optimization effort for $B_5$ using both the GA and GS algorithms, respectively. Note that we intentionally present the variable of joint $W_0$ which expectedly requires a low amount of torque to be operated (Fig. 3c). The optimal values of the variables (B's and C's) are listed in Table 5.

As discussed earlier, the GS scheme reveals the scatter-search pattern although converges to both the optimal values of variables and cost function satisfying the tolerances defined in Section 4; we validate the crucial issue of convergence by presenting the convergence histories. Figure 4 presents considerable computational costs (iterations) of 20400 and 87560 for both the GA and GS schemes, respectively, which look logical with respect to the scale of the coupled dynamic equations. Note that we have spent the significant computational times of 11855 and 58020 s for the GA and GS algorithms, respectively, which undoubtedly need to be minimized using the so-called step size analysis.

**Fig. 10** The experimental nominal and optimal trajectories using both the GA and GS algorithms (check our DSCL website) in sample times of **a** $t = 2$s, **b** $t = 5$s, **c** $t = 6$s, and **d** $t = 7$s; at $t = 7$s the robot's end effector through the nominal trajectory collides with the target object while the optimal one avoids such a collision throughout the whole operational time. The shadow frames present the nominal trajectory

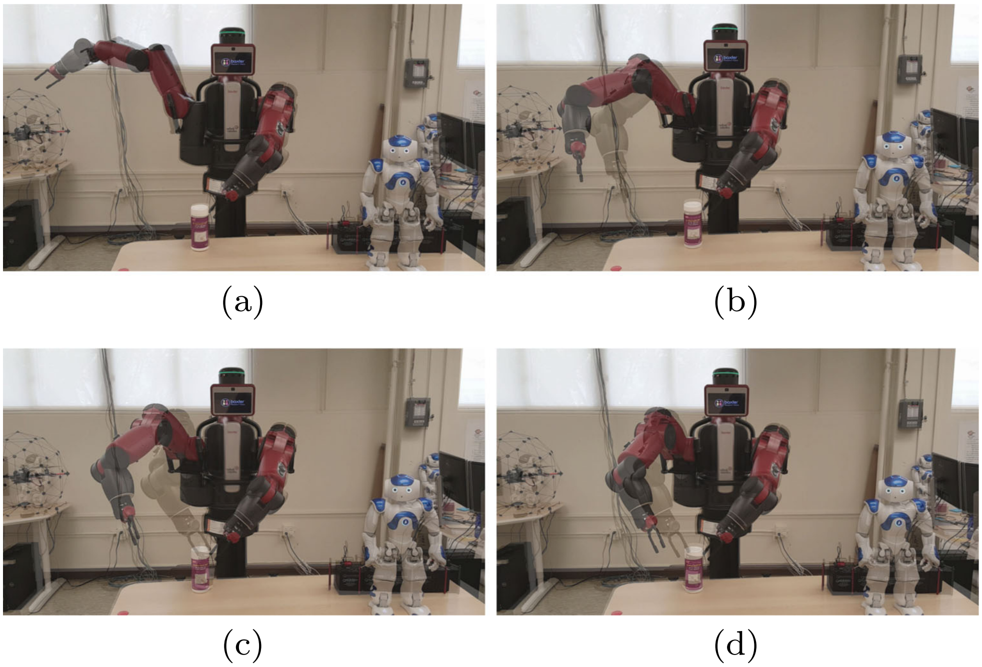

It is straightforward to observe that, based on the nominal and optimal variables listed in Tables 4 and 5, the optimal values of $B_1$, $B_3$, $B_6$, and $B_7$ are lower than the nominal ones. Note that the optimal values of $C_1$ and $C_7$, and $C_3$ and $C_6$ are smaller and higher than the nominal values, respectively. Shown in Figs. 5a, c and 6c, d reveal the effects of such optimal values of the $B_i$ and $C_i$ (i = 1, 3, 6, 7) on the trajectories of joints $S_0$, $E_0$, $W_1$, and $W_2$, respectively. The optimal angular velocities of joints $S_0$, $W_1$, and $W_2$ are lower than those of the nominal ones, as expected, leading to slower motions of the joints. Note that the joint $S_0$ takes the biggest share (Fig. 3a) among the other ones to consume the lumped amount of energy and therefore, its lower angular velocity would lead to a lower amount of the cost function defined.

Note that the optimal values of $B_2$, $B_4$, and $B_5$ are higher than those of the nominal ones, except $B_4$ of the GS method, and their corresponding C's have also higher values than the nominal C's. The effects of such higher values of the $B_i$ and $C_i$ (i = 2, 4, 5) can be visualized in Figs. 5b and 6a, b by presenting faster angular velocities of the optimal trajectories than the nominal ones. Note that we can easily conclude that the joint $E_1$, for both the nominal and optimal cases with respect to its small range of operation ($\theta_{E1} \leq 3.5°$), considerably spends a lower amount of energy in comparison with the other joints, particularly than that of the joint $S_0$ which we have previously addressed. Logically, the smooth optimized motions shown in Figs. 5a and 6d, despite the robot's nominal jerky trajectories, would expectedly demand lower driving torques to be used in the robot operation.

The negligible differences between the GA and GS schemes (Figs. 5a and 6d) are expected to be observed as they utilize different algorithms discussed in Section 4.

An interesting trade-off can be observed among the optimal values of B's and C's with respect to their subsequent effects on the optimal trajectories, which expectedly lead to both the lower angular velocities of the joints and energy consumption. A crucial issue of sensitivity of the optimization process to the variables of B's and C's hence needs to be carefully addressed. We discussed that even getting the higher values of C's, for the joints $E_0$ and $W_1$, yields almost the same nominal and optimal motions of the joints. Therefore, the roles of B's seem to be more drastic than the C's. A global sensitivity analysis has to be carried out in order to examine the roles of B's and C's on the optimization process.

**Fig. 11** The numerical step size (SS) analysis for the gradient-based algorithm (Global Search). **a** SS = $10^{-8}$ (default value). **b** SS = $10^{-7}$. **c** SS = $10^{-6}$. **d** SS = $10^{-5}$

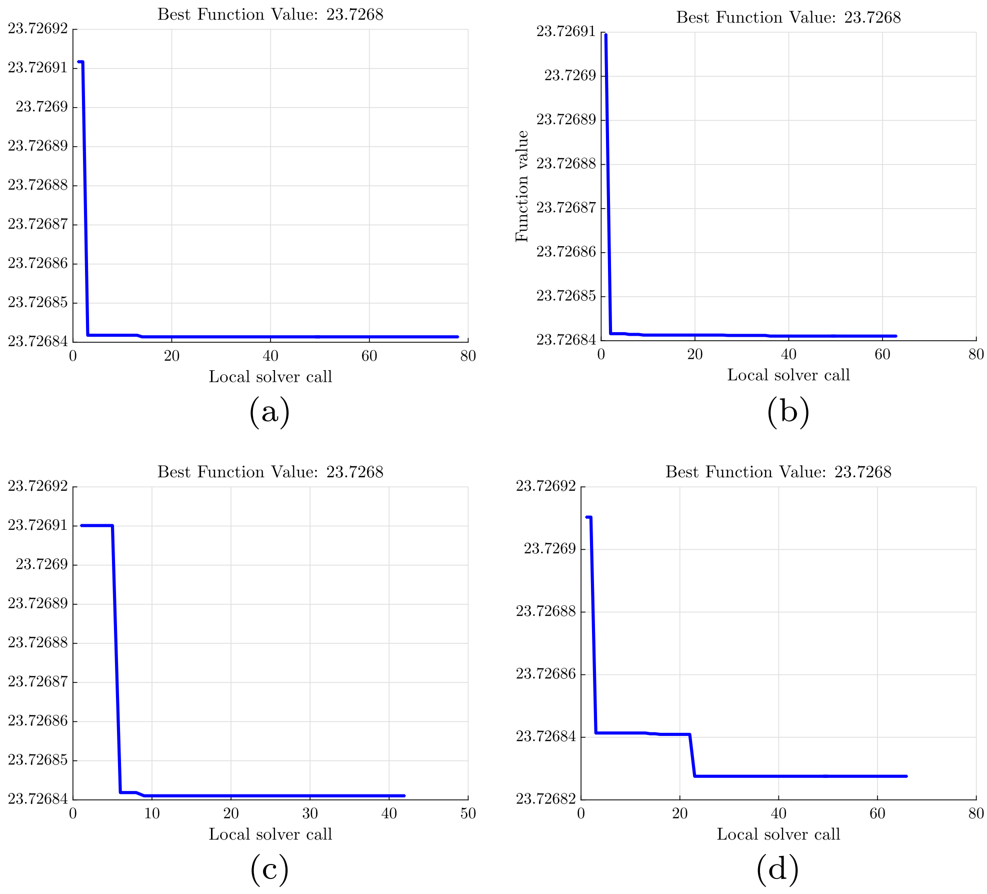

Typically, the local and global sensitivity analyses are used in determining the effects of changes of the optimization variables on the cost function defined. The local sensitivity analysis (one-at-a-time (OAT) method) evaluates the effect of one variable on the cost function at a time while keeping the other variables constant. Although the global sensitivity analysis utilizes set of random samples to search the design space with respect to the bounds defined. The global analysis would be an efficient approach as the change of each variable affects the dynamic characteristics of all the joints/links, through the interconnected dynamic equations, and subsequently the lumped cost function.

To carry out the global sensitivity analysis, we need to numerically calculate the gradient of the cost function with respect to the optimization variables as follows:

$$\nabla E = \left[ \frac{\partial E}{\partial B_i}, \frac{\partial E}{\partial C_i} \right]^T \quad i = 1, \cdots, 7$$

Shown in Figs. 7a and 8g are the results of such a sensitivity analysis. It is straightforward to conclude that the changes of B's significantly affect the cost function in comparison with the C's variations such that the gradient of the lumped energy consumption is too sensitive to the B's. It is also of a great interest to observe that the changes of $B_1$ and $B_2$, as expected, have drastic roles on the variations of the cost function and subsequently the optimization process (Fig. 7a, b). The physical interpretation of such dominant variables of $B_1$ and $B_2$ can be explained through the dynamics of the robot while, as discussed earlier, the joints $S_0$ and $S_1$ take the biggest shares of the torques needed to be applied. Therefore, we expect to observe the high sensitivity of the cost function to both the $B_1$ and $B_2$.

Shown in Fig. 9a, b are the energy consumptions minimized using both the GA and GS algorithms, respectively. Note that we have employed the heuristic and gradient-based methods to examine the locality/globality of the cost function minima. Figure 9a, b reveals a negligible difference (less than 0.05%) for the energy savings of both the schemes as follows:

$$\Delta E_{GS} = \frac{\overbrace{E_{nominal}}^{29.771(\text{J})} - \overbrace{E_{optimal}}^{23.7268(\text{J})}}{E_{nominal}} \times 100 = 20.03\% \tag{21}$$

$$\Delta E_{GA} = \frac{\overbrace{E_{nominal}}^{29.771(\text{J})} - \overbrace{E_{optimal}}^{23.7338(\text{J})}}{E_{nominal}} \times 100 = 20.027\% \tag{22}$$

The negligible higher amount of energy saving of the GS method can be justified through its corresponding optimal

**Fig. 12** The numerical step size (SS) analysis for the gradient-based algorithm (Global Search). **a** SS = $10^{-4}$. **b** SS = $10^{-3}$. **c** SS = $10^{-2}$

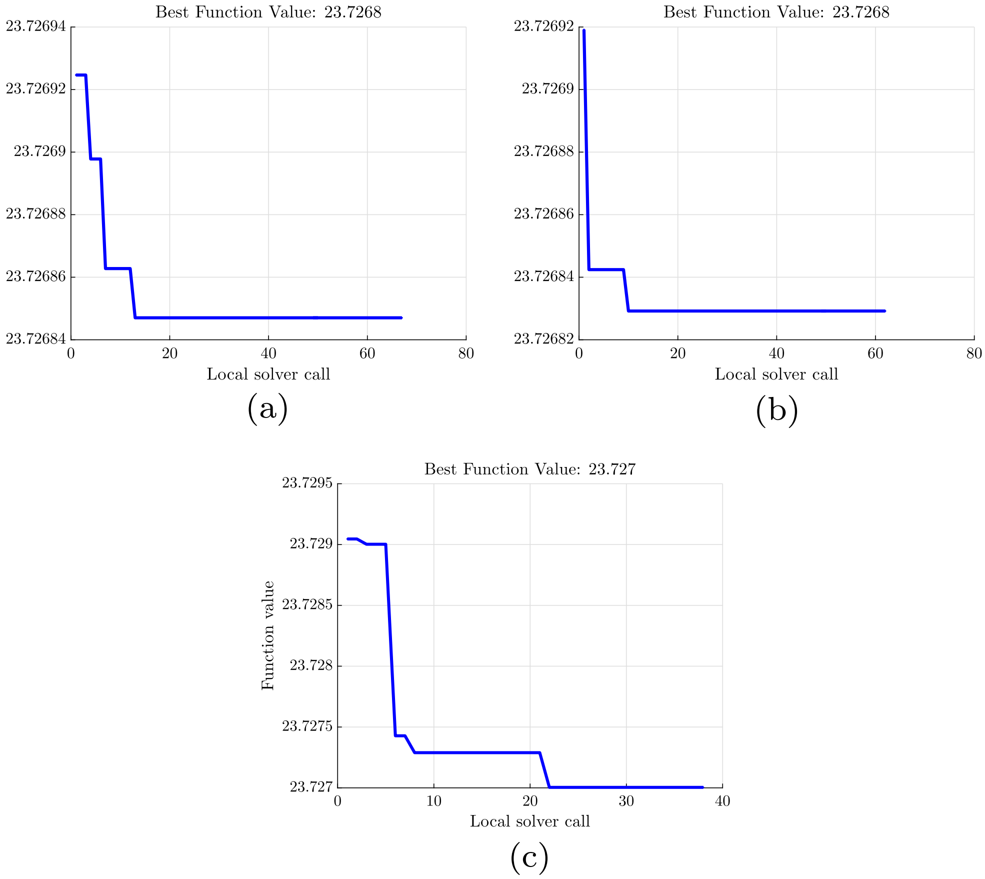

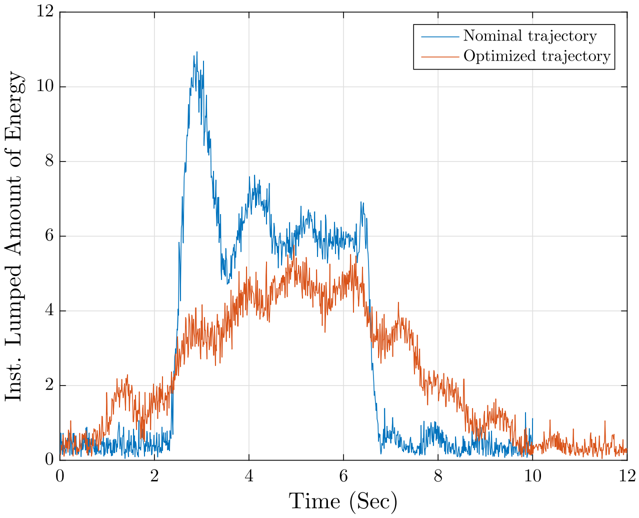

**Fig. 13** The experimental nominal and optimal instantaneous lumped amount of energy consumed in the joints

values of B's. We have previously discussed the significant roles of B's on the variation of the cost function via the global sensitivity analysis.

We have carried out experimental validation of the nonlinear analytical approach examining both the nominal and optimal trajectories. Figure 10a, d presents the experimental work, for sample operation times of 2s, 5s, 6s, and 7s, revealing smoother and slower motions of the joints/links for the optimal path than the nominal one. The jerky motion of the nominal trajectory caused an undesirable collision between the robot's end effector and the target object which needs to be smoothly picked up. It is interesting to observe that at $t = 7$s the robot's end effector through the nominal trajectory collides with the target object while the optimal one avoids such a collision throughout the whole operational time. Note that the shadow motions/frames stand for the nominal operation. The AVI files of the experiment are accessible via our **Dynamic Systems and Control Laboratory (DSCL)** website. Note that the difference between the energy savings of both the theoretical and experimental approaches is almost zero (Figs. 11 and 12):

$$\Delta E_{saving} = \frac{\overbrace{E_{theory}}^{23.7268(\mathrm{J})} - \overbrace{E_{experiment}}^{23.7224(\mathrm{J})}}{E_{theory}} \times 100 \approx 0\% \qquad (23)$$

Figure 13 presents the experimental nominal and optimal instantaneous lumped amount of energy consumed in the joints validating the optimization efforts shown in Fig. 9.

Shown in Figs. 4 and 9 reveal cumbersome computational costs (iterations), in particular for the GS method. The step size (SS) analysis is a necessity to be implemented in determining an optimal step size to reduce the computational cost/time and possibly the lumped amount of energy consumed.

Figures 11a and 12c present convergence histories of the GS method vs. different step sizes of SS $= 10^{-8}$ (default value) to SS $= 10^{-2}$. Shown in Fig. 14a reveals the decremental computational cost using the incremental values of the step size. Note that the minimal computational cost is obtained at SS $= 10^{-2}$ which yields upward of 80% reduction of the iteration. It is interesting to observe that the iteration increases for SS $= 10^{-5}$. From another aspect, the effect of the step size has to be evaluated for the cost function defined. Figure 14b presents a negligible decrease for the lumped amount of energy saved (less than $8.5 \times 10^{-4}$ %) using the step size of SS $= 10^{-2}$, which yielded the minimal computational cost. Therefore, it is straightforward to conclude that the step size of SS $= 10^{-2}$ is an optimal value to reduce both the computational cost and time.

Note that the step size analysis shown in Figs. 11a–12c indicates the convergence of the GS scheme despite its scatter-search pattern which we have previously addressed in Section 4. Figure 15 also shows the convergence of the GA method (the best fitness value).

**Fig. 14** The numerical step size (SS) analysis. **a** Iteration vs. SS. **b** Minimized energy vs. SS

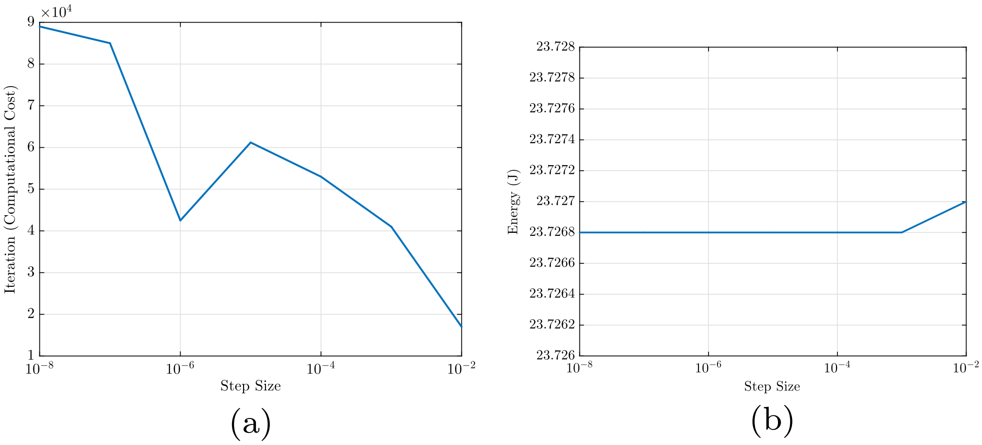

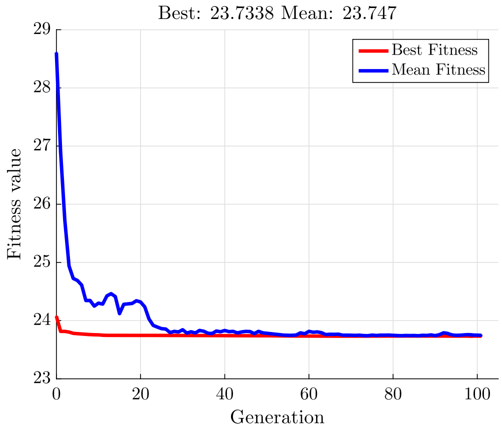

**Fig. 15** The convergence history of the GA algorithm

## 6 Conclusion

In this effort, we presented the interconnected trajectory optimization of a 7-DOF Baxter manipulator using both the heuristic and gradient-based methods to avoid being trapped in several possible local minima. The coupled dynamic equations of the robot were derived utilizing the Lagrangian method and then validated through the experimental work. We then optimized the joints' trajectories to generate smooth/efficient paths to avoid being exposed to the jerky motions of the nominal ones. The design sensitivity analysis was carried out to evaluate the effects of changes of the optimization variables on the cost function defined. As expected, the joints $S_0(B_1)$ and $S_1(B_2)$ play more significant roles on the optimization process than the other ones.

We have also carried out the experimental work, for both the nominal and optimal trajectories, to examine the accuracy of the analytical efforts. The step size analysis was performed to determine an optimal step size in order to reduce both the computational cost and time. We obtained the optimal step size of $SS = 10^{-2}$ which considerably reduced the computational cost (80%).

The principal results of this research work can be summarized as follows:

- A considerable amount of energy was saved (upward of 20%).
- The jerky motion and subsequently collision between the robot's end effector and the target object were removed using the optimized trajectory of the robot.
- An optimal step size resulted in the significant reductions of both the computational cost (upward of 80%) and time, in particular for the GS method.
- The experimental work validated the analytical approach by presenting almost no difference between the energy savings.

We are currently focusing our efforts on developing an adaptive controller (to be validated experimentally) to carry an unknown mass to a desired position using the optimal trajectory which we have developed here.

## References

1. Abu-Dakka FJ, Assad IF, Alkhdour RM, Abderahim M (2017) Statistical evaluation of an evolutionary algorithm for minimum time trajectory planning problem for industrial robots. Int J Adv Manuf Technol 89(1):389–406
2. Agarwal V (2012) Trajectory planning of redundant manipulator using fuzzy clustering method. Int J Adv Manuf Technol 61(5):727–744
3. Akbaripour H, Masehian E (2017) Semi-lazy probabilistic roadmap: a parameter-tuned, resilient and robust path planning method for manipulator robots. Int J Adv Manuf Technol 89(5):1401–1430
4. Al-taharwa I, Sheta A, Al-Weshah M (2008) A mobile robot path planning using genetic algorithm in static environment. J Comput Sci 4(4):341–344
5. Bagheri M, Ajoudani A, Lee J, Caldwell DG, Tsagarakis NG (2015) Kinematic analysis and design considerations for optimal base frame arrangement of humanoid shoulders. In: 2015 IEEE international conference on robotics and automation (ICRA). IEEE, pp 2710-2715
6. Bessonnet G, Lallemand JP (1994) On the optimization of robotic manipulator trajectories with bounded joint actuators or joint kinetic loads considered as control variables. J Dyn Sys Meas Control 116(4):819–826
7. Bobrow JE (1988) Optimal robot plant planning using the minimum-time criterion. IEEE J Robot Autom 4(4):443–450
8. Bobrow JE, Dubowsky S, Gibson JS (1985) Time-optimal control of robotic manipulators along specified paths. Int J Robot Res 4(3):3–17
9. Bryson JT, Jin X, Agrawal SK (2016) Optimal design of cable-driven manipulators using particle swarm optimization. ASME J Mech Robot 8(4):041,003–041,003–8
10. Chalvet V, Haddab Y, Lutz P (2015) Trajectory planning for micromanipulation with a nonredundant digital microrobot: shortest path algorithm optimization with a hypercube graph representation. ASME J Mech Robot 8(2):021,013–021,013–9
11. Chettibi T, Lehtihet H, Haddad M, Hanchi S (2004) Minimum cost trajectory planning for industrial robots. Eur J Mech A Solids 23(4):703–715
12. Costantinescu D, Croft EA (2000) Smooth and time-optimal trajectory planning for industrial manipulators along specified paths. J Robot Syst 17(5):233–249
13. Davidor Y (1991) Genetic algorithms and robotics: a heuristic strategy for optimization, vol 1. World Scientific
14. Funke LW, Schmiedeler JP, Zhao K (2015) Design of planar multi-degree-of-freedom morphing mechanisms. J Mech Robot 7(1):011,007
15. Garg DP, Kumar M (2002) Optimization techniques applied to multiple manipulators for path planning and torque minimization. Eng Appl Artif Intell 15(3):241–252
16. Gasparetto A, Lanzutti A, Vidoni R, Zanotto V (2011) Validation of minimum time-jerk algorithms for trajectory planning of industrial robots. ASME J Mech Robot 3(3):031,003–031,003–12
17. Hansen C, Kotlarski J, Ortmaier T (2013) Experimental validation of advanced minimum energy robot trajectory optimization. In: 2013 16th international conference on advanced robotics (ICAR). IEEE, pp 1–8
18. Hansen C, Kotlarski J, Ortmaier T (2013) Path planning approach for the amplification of electrical energy exchange in multi axis

robotic systems. In: 2013 IEEE international conference on mechatronics and automation (ICMA). IEEE, pp 44–50

19. Hopkins JK, Spranklin BW, Gupta SK (2011) A case study in optimization of gait and physical parameters for a snake-inspired robot based on a rectilinear gait. ASME J Mech Robot 3(1):014,503–014,503–5
20. Hsiao T, Weng MC (2013) Robust joint position feedback control of robot manipulators. J Dyn Sys Meas Control 135(3):031,010–031,010–11
21. Huang P, Xu Y, Liang B (2006) Minimum-torque path planning of space robots using genetic algorithms. Int J Robot Automat 21(3):229–236
22. Jr OYC, Emmanuel G Collins J, Sharma A, Kopinsky R (2017) Using dynamics to consider torque constraints in manipulator planning with heavy loads. J Dyn Sys Meas Control 139(5):051,001–051,001–12
23. Korayem M, Ghariblu H, Basu A (2004) Maximum allowable load of mobile manipulators for two given end points of end effector. Int J Adv Manuf Technol 24(9):743–751
24. Korayem MH, Nikoobin A (2008) Maximum payload for flexible joint manipulators in point-to-point task using optimal control approach. Int J Adv Manuf Technol 38(9):1045–1060
25. Ma RR, Dollar AM (2013) Linkage-based analysis and optimization of an underactuated planar manipulator for in-hand manipulation. ASME J Mech Robot 6(1):011,002–011,002–9
26. Ma RR, Dollar AM (2014) Linkage-based analysis and optimization of an underactuated planar manipulator for in-hand manipulation. J Mech Robot 6(1):011,002
27. Mann MP, Zion B, Rubinstein D, Linker R, Shmulevich I (2014) Minimum time kinematic motions of a cartesian mobile manipulator for a fruit harvesting robot. J Dyn Sys Meas Control 136(5):051,009–051,009–9
28. Mattmuller J, Gisler D (2009) Calculating a near time-optimal jerk-constrained trajectory along a specified smooth path. Int J Adv Manufac Technol 45(9-10):1007–1016
29. Meike D, Ribickis L (2011) Energy efficient use of robotics in the automobile industry. In: 2011 15th international conference on advanced robotics (ICAR), pp 507–511
30. Meike D, Ribickis L (2011) Industrial robot path optimization approach with asynchronous fly-by in joint space. In: 2011 IEEE international symposium on industrial electronics (ISIE). IEEE, pp 911–915
31. Moberg S, Wernholt E, Hanssen S, Brogardh T (2014) Modeling and parameter estimation of robot manipulators using extended flexible joint models. J Dyn Sys Meas Control 136(3):031,005–031,005–13
32. Muller A (2004) Energy optimal control of serial manipulators avoiding collisions. In: Proceedings of the IEEE international conference on mechatronics. IEEE, pp 299–304
33. Naseradinmousavi P (2015) A novel nonlinear modeling and dynamic analysis of solenoid actuated butterfly valves coupled in series. ASME J Dyn Syst Meas Control 137(1):014,505–014,505–5
34. Naseradinmousavi P, Krstic M, Nataraj C (2016) Design optimization of dynamically coupled actuated butterfly valves subject to a sudden contraction. ASME J Mech Des 138(4):041,402–041,402–11
35. Naseradinmousavi P, Segala DB, Nataraj C (2016) Chaotic and hyperchaotic dynamics of smart valves system subject to a sudden contraction. ASME J Comput Nonlinear Dynam 11(5):051,025–051,025–9
36. Naseradinmousavi P, Machiani SG, Ayoubi MA, Nataraj C (2017) Coupled operational optimization of smart valve system subject to different approach angles of a pipe contraction. J Struct Multidiscip Optim 55(3):1001–1015. doi:10.1007/s00158-016-1554-7
37. Paryanto BrossogM, Bornschlegl M, Franke J (2015) Reducing the energy consumption of industrial robots in manufacturing systems. Int J Adv Manuf Technol 78(5):1315–1328
38. Pfeiffer F, Johanni R (1987) A concept for manipulator trajectory planning. IEEE J Robot Autom 3(2):115–123
39. Ramabalan S, Saravanan R, Balamurugan C (2009) Multi-objective dynamic optimal trajectory planning of robot manipulators in the presence of obstacles. Int J Adv Manuf Technol 41(5):580–594
40. Rubio F, Valero F, Sunyer J, Cuadrado J (2012) Optimal time trajectories for industrial robots with torque, power, jerk and energy consumed constraints. Ind Robot Int J 39(1):92–100
41. Rubio F, Llopis-Albert C, Valero F, Suner JL (2016) Industrial robot efficient trajectory generation without collision through the evolution of the optimal trajectory. Robot Auton Syst 86:106–112
42. Saravanan R, Ramabalan S, Balamurugan C (2008) Evolutionary collision-free optimal trajectory planning for intelligent robots. Int J Adv Manuf Technol 36(11):1234–1251
43. Schmidt B, Mohammed A, Wang L (2013) Minimising energy consumption for robot arm movement. In: NEWTECH 2013 the 3rd international conference on advanced manufacturing engineering and technologies. Sweden, pp 125–134
44. Seriani S, Gallina P, Gasparetto A (2014) A performance index for planar repetitive workspace robots. J Mech Robot 6(3):031,005
45. Shiller Z (1996) Time-energy optimal control of articulated systems with geometric path constraints. J Dyn Syst Meas Control 118(1):139–143
46. Shiller Z, Lu HH (1992) Computation of path constrained time optimal motions with dynamic singularities. J Dyn Syst Meas Control 114(1):34–40
47. Spong MW, Hutchinson S, Vidyasagar M (2005) Robot modeling and control. Wiley
48. Tang GR, Mooring BW (1992) Plane-motion approach to manipulator calibration. Int J Adv Manuf Technol 7(1):21–28
49. Thiede S (2012) Energy efficiency in manufacturing systems. Springer Science & Business Media
50. Tran TV, Wang Y, Ao H, Truong TK (2015) Sliding mode control based on chemical reaction optimization and radial basis functional link net for de-icing robot manipulator. J Dyn Sys Meas Control 137(5):051,009–051,009–16
51. Verscheure D, Demeulenaere B, Swevers J, Schutter JD, Diehl M (2008) Time-energy optimal path tracking for robots: a numerically efficient optimization approach. In: 10th IEEE international workshop on advanced motion control. IEEE, pp 727–732
52. Vukobratovic M, Kircanski M (1982) A method for optimal synthesis of manipulation robot trajectories. J Dyn Sys Meas Control 104(2):188–193
53. Yu X, Zhao Y, Wang C, Tomizuka M (2016) Trajectory planning for robot manipulators considering kinematic constraints using probabilistic roadmap approach. J Dyn Sys Meas Control 139(2):021,001–021,001–8
54. Zhang Y, Ge SS, Lee TH (2004) A unified quadratic-programming-based dynamical system approach to joint torque optimization of physically constrained redundant manipulators. IEEE Trans Syst Man Cybern B Cybern 34(5):2126–2132
55. Zhang Z, Zhang Y (2012) Repetitive motion planning and control on redundant robot manipulators with push-rod-type joints. J Dyn Sys Meas Control 135(2):024,502–024,502–4
56. Zhao K, Schmiedeler JP (2016) Using rigid-body mechanism topologies to design path generating compliant mechanisms. J Mech Robot 8(1):014,506
57. Zhao Y, Huang T, Yang Z (2007) A successive approximation algorithm for the inverse position analysis of the general serial manipulators. Int J Adv Manuf Technol 31(9):1021–1027